

Investigating the influence of bending stiffness and processing parameters on single-leg bending geometries of additively manufactured composites

Stiller T., Kerschbaumer R.C., Waly C., Zink Béla, Slapnik J., Pinter G.

This accepted author manuscript is copyrighted and published by Elsevier. It is posted here by agreement between Elsevier and MTA. The definitive version of the text was subsequently published in [Results in Engineering, 24, 2024, DOI:

[10.1016/j.rineng.2024.103276](https://doi.org/10.1016/j.rineng.2024.103276)]. Available under license CC-BY-NC-ND.



Research paper



# Investigating the influence of bending stiffness and processing parameters on single-leg bending geometries of additively manufactured composites

T. Stiller<sup>a,b,\*</sup>, R.C. Kerschbaumer<sup>a</sup>, C. Waly<sup>b</sup>, B. Zink<sup>c</sup>, J. Slapnik<sup>d</sup>, G. Pinter<sup>b</sup>

<sup>a</sup> Polymer Competence Center Leoben GmbH, Sauraugasse 1, 8700 Leoben, Austria

<sup>b</sup> Department of Polymer Engineering and Science, Material Science and Testing of Polymers, Montanuniversitaet Leoben, Franz-Josef Straße 18, 8700 Leoben, Austria

<sup>c</sup> Department of Polymer Engineering, Faculty of Mechanical Engineering, Budapest University of Technology and Economics, Műegyetem rkp. 3., H-1111 Budapest, Hungary

<sup>d</sup> Faculty of Polymer Technology, Ozare 19, 2380 Slovenj Gradec, Slovenia

## ARTICLE INFO

### Keywords:

Additive manufacturing  
Polymers  
Multi-material  
Single leg bending  
Bonding strength

## ABSTRACT

In less than a decade, additive manufacturing technologies have been developed so successfully that they already produce small and medium-sized lot sizes of prototypes or customised components in the industry. With its new possibilities such as combining materials and technologies, the benefits of different technologies can be merged and broaden future application fields. One way is to print with one technology on a part produced by another. Thus, a thermally bonded part composed of, e.g., selectively sintered and material-extruded components can be created. This combination of technologies was considered in this study to investigate the bonding strength of extrusion-based layers on selectively sintered surfaces and the impact of nozzle temperature, orientation, and thickness of imprinted materials. The extrusion-based layers covered stiff (fibre-reinforced polyamide) and soft (thermoplastic polyurethane) material properties with pre-cracked single-leg bending (SLB) specimens to study their effect on delamination tendencies. This combination of materials and additive manufacturing technologies has not yet been studied for the SLB testing method. The scope of this study is to obtain more information on how relatively hard-hard and hard-soft combinations behave for this special testing method. The results of this testing method were evaluated using two different fracture mechanical approaches to determine the energy release rate. A clear trend towards an improved bonding, thus, higher values, was found for higher nozzle temperatures. Furthermore, a limitation regarding the required bending stiffness of the composites was found. Overall, the single-leg bending testing method enables a relative ranking for material combinations with a certain bending stiffness.

## 1. Introduction

In 1989, S. Scott Crump filed a patent titled “Apparatus and method for creating three-dimensional objects” – the invention of a 3D printer [1]. With the expiration in 2006, the RepRap printers flooded the market and made additive manufacturing available for everybody, leading to a rapid increase in developments and numbers for additive manufacturing methods. Including all material classes (metals, ceramics, and polymers) there are seven process categories according to the ISO ASTM 52900:2021 in additive manufacturing: binder jetting (BJT), directed energy deposition (DED), material extrusion (MEX), material jetting (MJT), powder bed fusion (PBF), sheet lamination (SHL), and vat polymerisation (VPP) [2].

A lot of research was conducted for MEX and selective laser sintering (SLS), a subcategory of PBF, in the last years to optimise the material [3–6], the process parameters [7,8], the part quality [9,10], new application fields [11–17], and also the recycling of the leftover powder [18–21] or filament [22–24]. Especially for MEX, a crucial factor defining the part quality is the bonding strength between and in the layers. One important factor is the neck formation, which represents the contact area between deposited paths after fusing and its quality defines the bonding strength. Investigations about this neck formation and the bonding strength were quantified by tensile tests [8,25,26], bending tests [26–28], trouser tear tests [29] or double cantilever beam (DCB) tests [30–32]. Generally, a higher percentage of infill (amount of material printed inside of the perimeter) enhances the bonding, but at the

\* Corresponding author at: Department of Polymer Engineering and Science, Material Science and Testing of Polymers, Montanuniversitaet Leoben, Franz-Josef Straße 18, 8700 Leoben, Austria

E-mail addresses: [tanja.stiller@stud.unileoben.ac.at](mailto:tanja.stiller@stud.unileoben.ac.at), [tanja.stiller@pccl.at](mailto:tanja.stiller@pccl.at) (T. Stiller).

<https://doi.org/10.1016/j.rineng.2024.103276>

Received 9 August 2024; Received in revised form 3 October 2024; Accepted 28 October 2024

Available online 30 October 2024

2590-1230/© 2024 The Author(s). Published by Elsevier B.V. This is an open access article under the CC BY license (<http://creativecommons.org/licenses/by/4.0/>).

same time, the weight reduction effect is lost [33,34]. Therefore, a compromise between sufficient bonding and limiting the material use has to be found for each application case.

With the development of printers, it is already possible to print different colours or even materials simultaneously on one printer [35, 36]. For the progress in technology, a combination of materials opens up a new path for properties, such as metamaterials or a reduction in processing steps [13,14,26,27,37]. Multi-material prints for MEX require a sufficient bonding between the layers and the single materials. Different studies have focussed already on the bonding strength of different material groups [38–41] or the same matrix material with different reinforcements [8,30,32,42]. Slapnik et al. [38] investigated the bonding strength of thermoplastic polyurethane (TPU) printed on injection moulded polyamide surfaces with a special pull of test setup. This gives a quantitative ranking for the impact of processing and part factors for a quasi-static property. A tensile test is the most popular characterisation method for polymers, but it does not always represent the real loading scenario. In application, many parts are exposed to bending, shear, cyclic load or even a combination of them. With a modification of soft-hard components, the failure mechanism can change drastically for the same loading case as shown in [43]. This consequence can also be utilized to their benefit, for example by combining stiff materials with a soft interlayer in a sandwich structure, which acts as a crack-arresting layer, to prevent catastrophic failure [44]. Such combinations become of more interest for engineering applications. In the case of present cracks, the fracture mechanical approaches give more information about the lifetime and durability of the bonding layers. Khudiakova et al. applied a fracture mechanical approach by testing the bonding strength with crack round beams (CRB) [42]. A clear difference was found for the single combinations. Another approach was by single leg bending (SLB), as it was shown by Rabbi et al. [39]. They printed Nylon (polyamide 6.6) on polylactic acid (PLA) and tested different processing parameters with this mixed-mode testing setup. The evaluation and test are based on Davidson's calculations and applicable to a composite consisting of two different material types [45]. Their material combination was successfully tested and correlations between the results and the applied printing parameters were found. More authors proposed equations on how to evaluate this mixed mode I/II loading scenario, which was tested on rather stiff (bulk) materials, adhesives, or numerical simulations [46–52]. Nevertheless, these studies focus on a stiff-stiff material combination manufactured by the same technology, for which the utilized approaches are applicable. So far it has not been investigated yet if and how the SLB-geometry works for soft-hard material combinations for different AM-technologies.

With the increasing demand for combining properties in one component, which are mutually exclusive, the fabrication of multi-

materials become more important. By the production of a layered composite the question of the bonding strength and quality rises. This study deals with the effect of material combinations, which were produced by different AM technologies, and their mechanical response to bending loads with a pre-crack. The additional aim is to determine the impact of processing parameters and bending stiffness on the required energy to separate two materials following the single-leg bending test setup. To cover different mechanical property ranges, SLS-powder (polyamide 12) was imprinted with fibre-reinforced polyamides (with coated glass fibres and carbon fibres) as well as with TPU, a soft thermoplastic elastomer-based polyurethane with high flexibility. It was studied, how the bending stiffness (i.e., thickness of each material) impacts the results and the crack propagation as well as how printing parameters such as nozzle temperature and orientation of the bonding layer affect the results.

## 2. Experimental

### a. Materials & printing details

Within this study, two types of technologies were combined, namely SLS and MEX. Samples produced with SLS were sintered on a Farsoon SS403P produced by DISTech (Disruptive Technologies GmbH, Kapfenberg, Austria), whereas MEX-samples were printed either on a Makerbot Method X (MakerBot Industries, LLC, New York City, USA) or using a Qidi Xmax (QIDI Technology, Wenzhou, Zhejiang, China). For the SLS samples, commercially available PA 12 powder was used and for the MEX samples, different filament materials were studied. The selection covers hard/brittle (fibre-reinforced PA 12) and soft/ductile filaments (thermoplastic polyurethane (TPU)). Details about the materials and the printing parameters are summarised in Table 1. All MEX parts were printed in an alternating 0°/90° infill pattern to avoid warpage. For all utilized printers, the bed temperature was set to 60 °C in a closed chamber. Generally, similar polymers bond to each other, therefore, the selection was made for the fibre-reinforced PA 12 filaments (nickel-coated glass fibre-reinforced (PAGF with 20 wt.% glass fibres) and carbon fibre-reinforced (PACF with 15 wt.% carbon fibres)) and by previously conducted studies it was found that TPU also adheres sufficiently to polyamide [38]. All filaments were dried only before printing at 70 °C for at least 8 h in an oven without vacuum. As it is recommended by the producer, PACF was annealed after printing for 24 h at 70 °C. Its extent on the flexural properties was investigated by comparing annealed and not annealed PACF specimens, for SLB measurements only annealed PACF samples were considered. In general, the processing parameters were chosen empirically in a range where the print gave an optically satisfactory result for all combinations.

**Table 1**  
Material and printing information for all investigated materials.

Name	PA 12	PAGF	PACF	TPU
Technology	SLS	MEX	MEX	MEX
Tradename (Producer)	ALM PA 650 (Advanced laser materials)	Lastik C/XEL-W (CAS)	Qidi PA 12 CF15 (Qidi)	TPU flex hard (Extrudr)
Printer	Farsoon SS403P	Makerbot Method X	Makerbot Method X	Qidi Xmax
Powder* / Bed / Nozzle temperature	≈ 174 °C No nozzle	60 °C 230 °C; 250 °C	60 °C 250 °C	60 °C 230 °C; 250 °C
Printing speed	≈ 12,500 mm/s	50 mm/s	50 mm/s	20 mm/s
Infill	Linear	Linear (80%)	Linear (80%)	Linear (80%)
Infill angle		0° / 90°	0° / 90°	0° / 90°
Contour	1 perimeter	1 perimeter	1 perimeter	2 perimeters
Layer height	0.12 mm	0.2 mm	0.2 mm	0.2 mm
Testing of	None (no variation)	Nozzle temperature; Sample thickness; Orientation	Sample thickness; Orientation	Nozzle temperature; Sample thickness; Orientation

\* for SLS-produced parts.

### b. Sample geometries and preparation

To investigate the properties of thermal and flexural behaviour as well as the bonding strength, the geometries and the sample's preparation varied between the different methods. In the following, it will be distinguished between mono and mixed materials, where mono represents a sample produced with only one material and mixed represents a MEX structure printed onto an SLS plate.

Mixed samples were produced by printing MEX material onto the SLS substrate, this order was not changed. To produce the samples, an SLS plate was fixed on the printing bed as shown in Fig. 1a) with a double-sided scotch tape below. In the beginning, the G-code was programmed to have a z-off-set equal to the thickness of the plate and starts, therefore, to print on the SLS surface. A polyimide tape at the lower part fulfils two jobs in one: it hinders the sample from moving and at the same time it defines the initial crack position. The distance between the outer edge and the initial crack was about 25 mm, but the real initial crack length was measured precisely after the delamination. This was done by measuring the distance between the support and the position of the initial crack from the images obtained during testing. The tape covered the whole width of the samples and was 15 mm to 20 mm broad to ensure the initial crack. Protruding SLS parts, as visible in Fig. 1b), were considered in the later calculations to simplify the production. By changing the thickness between the SLS plate and the MEX layers, the impact on the bending stiffness was investigated. SLS plates were 2 mm to 4 mm thick, but 2 mm plates tended to warp after the imprinting of the MEX layers, which varied between 1 mm to 4 mm. In the following, the thickness will be labelled with "x\_y", where x represents the thickness of the SLS plate in mm and y the thickness of the MEX part in mm. Besides the nozzle temperature and the sample thickness, the orientation of the first layer, i.e. the bonding layer, was studied. In Fig. 1c) the orientations are schematically shown – horizontally orientated layers are parallel to the crack front, while vertically orientated layers are deposited perpendicular to it.

### c. Thermal characterisation

With Differential Scanning Calorimetry (DSC) the melting and crystallisation temperatures were determined. Samples of 7 – 10 mg were cut and put into a 40 µl aluminium crucible with a perforated lid. The procedure was conducted according to ISO 11,357-1 [53] on a "Mettler Toledo DSC 1 Star" system (Mettler – Toledo Inc., Greifensee, Switzerland). All measurements were done under a flooded nitrogen atmosphere with 50 ml/min, a heating rate of 10 K/min and the cooling cycle with a rate of 20 K/min. One DSC measurement consisted of two heating and one cooling step. The set temperature limits (25 °C and 250 °C) were held for 3 min before heating or cooling started. All samples of MEX materials were taken from the filament and the PA 12 SLS sample was cut out from an already sintered part. Of each material, at least three samples were measured.

### d. Mechanical and fracture mechanical characterisation

To determine the behaviour during a flexural load, 3-point bending tests were conducted according to ISO 178 [54] for different sample variations. All MEX samples were printed with a nozzle temperature of 250 °C. Each set of samples was stored and tested at laboratory conditions (23 °C, 50% r.H.) without any additional drying step. PA12 is significantly less hygroscopic than e.g. PA6, therefore, no additional drying step was conducted. Furthermore, testing of completely dry samples does not reflect conditions in reality and complicates the testing due to the brittle behaviour of fully dried SLS-based polyamide specimens [18]. All flexural tests were conducted on Zwick Z010 (Zwick Roell GmbH, Ulm, Germany) with a 500 N load cell, testing with a fin and support radius of 5 mm, a support distance of 64 mm, and a testing speed of 2 mm/min without switch over after the Young's modulus determination. Flexural properties were determined by five repetitions using the arithmetic mean value and the standard deviation.

To compare the bonding strength between SLS and MEX layers, samples like in Fig. 1b) were investigated by an SLB test setup. In principle, the sample is stressed by a 3-point bending load, but due to the sample's geometry and the pre-crack, a delamination between the layers can be provoked [44]. In general, the setup resembles an end-notched flexure test, but by a protrusion with only one material of the samples to one cushion, the crack grows by opening up (mainly mode I) and not by pure shear (mode II). Depending on the stiffness ratio and the deflection, at which the crack continues, there is either mode I or mixed mode I/II [45]. An image of the sample geometries is illustrated in Fig. 2a) and the test setup in Fig. 2b). The tests were performed at 0.5 mm/min without a switch point on a Zwick Z010 with a 500 N load cell at a 3-point bending setup with adapted heights for one support to balance the thickness difference. Both supports and the fin had a radius of 5 mm and the total distance between the supports was 114 mm (see Fig. 2b). All SLB tests were recorded during testing to analyse the crack growth and understand the underlying mechanisms. The tests were recorded with a mercury system (v2.8) with one Prosilica GT 6600 camera (Allied Vision Technologies GmbH, Stadtroda, Germany) and a macro lens Tokina with a 100 mm focal length (Kenkō Tokina, Shinjuku, Japan). Images obtained from the mercury system were taken to compare force-displacement curves with visible events, while the numerical evaluation was done with the data from the tensile machine. Further analysis of the samples and bonding surfaces was done on the light microscope Axioscope 5/7 (Carl Zeiss AG, Jena, Germany). In the results section, the arithmetic mean value of four tests with the standard deviations are given, if not stated otherwise. This sample number follows the recommended specimen amount from ISO13586 [55] and ASTM D5045 [56], both fracture mechanical procedures since no recommendation exists yet for this SLB test. Even by increasing the sample number, a scattering of the results is to be expected due to the fabrication process with additive manufacturing – in this case even a combination of two technologies.

Two evaluation methods were considered to calculate the energy release rate  $G$  for the conducted tests. With the basic energy-based evaluation of the test with Eq. (1), this method requires only



Fig. 1. (a) Position and fixture of the SLS plates, (b) ready to test SLB samples, and (c) orientations of the bonding layer.

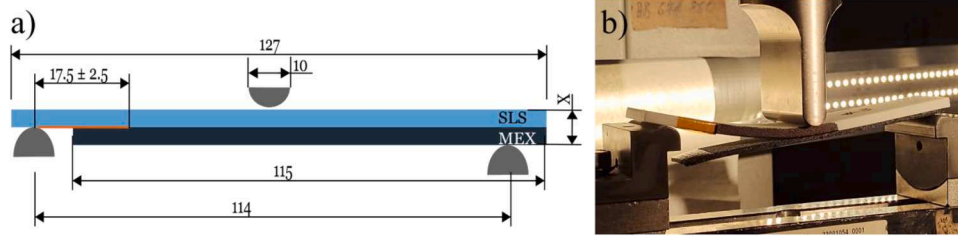


Fig. 2. (a) Geometry (X is 3, 4, 5, or 6; dimensions are in mm) and (b) test setup of an SLB-specimen.

information about the force-displacement curve and the geometry of the sample. This equation is based on homogenous bulk materials, which usually is utilized in LEFM (linear elastic fracture mechanics), but with boundary conditions such as the formation of a small plastic zone in front of the crack tip and linear elastic material behaviour. Nonetheless, it is applicable for this investigation since it was considered to calculate the energy at the initiation of the crack growth.

$$G_{U_c} = \frac{U_c}{bW} \quad (1)$$

In this equation,  $U_c$  is the crack initiation energy (area below force-displacement-curve),  $b$  is the width of the specimen, and  $W$  is the total sample length minus the initial crack length.

Another, more detailed, evaluation (Eq. (2)) was proposed by Davidson and Sundararaman [39,45] and is another fracture mechanical approach adapted for the SLB geometry of bonded dissimilar materials:

$$G_{SLB} = \frac{3P\delta a^2}{2b} \left[ \frac{R-1}{2L^3 + a^3(R-1)} \right] \quad (2)$$

Where  $P$  is the applied force before the crack grows,  $\delta$  is the load point displacement when the crack starts to grow,  $a$  is the initial crack length,  $b$  is the width of the specimen,  $R$  is the stiffness ratio (calculated by the bending rigidity of the uncracked in ratio to the top plate, and  $L$  is the mid-span length.  $R$  can be described as a function of the single material properties ( $E_1$  and  $E_2$ ) and their thickness ( $t_1$  and  $t_2$ ) to the top plate ( $E_T$  and  $t_T$ ), as shown in Eq. (3) [45].

$$R = \frac{D}{D_T} = \frac{D_{11} - \frac{B_{11}^2}{A_{11}}}{D_T} = \frac{\frac{(E_1 t_1 (t_1^2 + 3t_2^2) + E_2 t_2 (t_2^2 + 3t_1^2))}{12} - \frac{((E_2 - E_1) t_1 t_2)^2}{4(E_1 t_1 + E_2 t_2)}}{\frac{E_T t_T^3}{12}} \quad (3)$$

### 3. Results and discussion

#### a. Thermal characterisation

Within this study, all materials are semi-crystalline thermoplastics. To thermally bond chemically affine semi-crystalline thermoplastics without an adhesive or other external parameter (e.g. pressure, solvents) together, a polymer has to be above its melting peak temperature. In

Table 2

Onset temperatures and melting peak temperatures of the first and second heating cycles as well as of the cooling cycle for all single materials.

Material	1st heating		Cooling		2nd heating	
	T <sub>onset</sub> [°C]	T <sub>melting</sub> [°C]	T <sub>onset</sub> [°C]	T <sub>crystal</sub> [°C]	T <sub>onset</sub> [°C]	T <sub>melting</sub> [°C]
PA 12	173.1 ± 2.3	186.4 ± 2.9	145.6 ± 3.0	138.6 ± 3.4	169.4 ± 1.0	176.8 ± 1.8
PAGF	170.4 ± 2.0	179.4 ± 0.2	162.9 ± 0.2	158.0 ± 0.5	170.9 ± 0.6	178.2 ± 0.6
PACF	198.8 ± 3.1	207.6 ± 0.7	173.3 ± 0.8	163.3 ± 2.1	179.8 ± 0.7	192.3 ± 0.3
TPU	194.4 ± 0.7	205.8 ± 0.5	172.1 ± 1.4	162.6 ± 2.7	199.5 ± 1.3	220.1 ± 2.7

Table 2 the onset temperatures and the peak temperature of heating and melting are listed. Regarding the printing, the first heating cycle represents the actual condition better, but this cycle is influenced by thermal and mechanical history as well as the contact area in the crucible (round filament violates the requirement of a flat contact area for optimal heat conductivity). Therefore, also the second heating cycle was considered since it represents the material properties after the thermal and mechanical history has been “deleted”. Differences in the heating cycles originate from the different cooling histories, with the first one being the production cooling (e.g. water bath or air cooling after filament extrusion) and the second one from the defined cooling during the DSC measurement. While all PA samples showed a decrease in the melting peak temperature for the second heating, TPU showed a higher temperature. This is due to specific composition with hard and soft segments of TPU, which creates chemical bonds, but also reversible physical bonds. With the defined cooling cycle, the hard phase with crystals formed different amounts of the crystal structure (type I and type II) and post-crystallisation reactions during the first heating cycle are not excluded [57,58]. For the MEX materials, which were printed on the SLS parts, the nozzle temperature was set to 230 °C or 250 °C. The melt itself reaches temperatures a bit below the set nozzle temperature to ensure printability [59,60]. Polymers have a high specific heat capacity (e.g. PA 12  $c_p \approx 2.6 \text{ J g}^{-1} \text{ K}^{-1}$  at 500 K [61]), which cools down slower and is therefore helpful for thermal bonding since the deposited filament radiates heat and has more time to bond to the lower surface [59,62]. In the case of high-temperature melting materials which are imprinted with a low-temperature melting filament, the bonding will most likely not be sufficient and delaminate during the cooling process. Additionally, the chemical affinity has to be high enough to enable adhesive forces in the bonding layer [63]. Higher temperatures would improve the bonding, but, simultaneously, worsen the printability due to too low viscosity [26]. Furthermore, too high temperatures in the nozzle can cause irreversible thermal damage to the polymer melt. On the other side, too low temperatures will not create the desired bonding between the layers.

#### b. Mechanical characterisation – flexural properties

For the subsequent fracture mechanical methods, the Young’s modulus of each material is required to calculate the bending stiffness of the composites. 3-point bending tests were conducted, since they represent the subsequent loading during SLB, and are summarised in Table 3. As expected, Young’s moduli of fibre-reinforced PAs (PAGF and PACF) are significantly higher than SLS-based PA 12 and TPU [64,65].

Table 3

Young’s modulus and flexural strength of the investigated materials.

Material	Young’s modulus [MPa]	Flexural strength [MPa]
PA 12	1436 ± 140	61 ± 5
PAGF	3253 ± 120	40 ± 2
PACF	2830 ± 150	64 ± 1
PACF (annealed)	3656 ± 235	78 ± 5
TPU	150 ± 4	5 ± 1

Generally, it has to be mentioned that the printing orientation and the orientation of the load application have an enormous effect on the properties [34,66,67]. It was neglected because the specimens were printed in an alternating orientation of  $0^\circ$  and  $90^\circ$  throughout the height. Nonetheless, the orientation of the first and last layers has an impact on the failure mechanism of the flexural samples [43,68]. It has to be mentioned that the mechanical properties can be influenced by the processing parameters, such as nozzle/bed/chamber temperature, printing speed, infill degree and pattern by changing the porosity, the quality of neck formation, morphology in the bonding layer, and chain entanglements – which was studied in detail in the literature [26,69,70]. Higher temperatures enable a better neck formation and, thus, a better fusion of the layers. Further influencing factors are the environmental conditions, especially humidity and temperature. Both are known to affect the mechanical properties of polyamides, but PA 12 is less affected than e.g. PA 6 [61,71–73].

Investigations on the SLS/MEX composites were not included, since they strongly depend on the bonding strength between the materials and their stiffness. Testing mixed flexural specimens (with SLS and MEX), resulted in all cases in a premature failure in the bonding layer, which was not the purpose of the flexural test. If the bonding between dissimilar materials is too weak for the shear at the half height of the specimen, the composite delaminates and only the freely deformable and moveable layers are tested, as visible in Fig. 3. In the same image, the relative shift of MEX to SLS is visible at the ends of the specimen, which shows a protrusion of the MEX layer. Inside a composite, the stress changes according to the different stiffness values of each layer, but the deformation is in an ideal case linear over the specimen thickness for sufficient bonding. If the difference in stress or the shear (in the middle of the sample height) is too high for the bonding, it will fail [43, 74]. Therefore, the bending stiffness of the composite was calculated based on the geometry and the stiffness of each material.

### c. Fracture mechanical characterisation – single-leg bending

For the characterisation using the SLB test set-up four material combinations (PA 12 with PAGF, PACF, or TPU and PACF mono), were investigated regarding nozzle temperature, thickness ratio and orientation of the bonding layer. First, the stiffer fibre-reinforced PAGF and PACF will be discussed. PA 12/PAGF was tested for different parameters showing the first critical parameters, while PA 12/PACF and PACF mono will be studied on the thickness ratio. With the knowledge of these stiff combinations, the question arises, of how the sample geometry works out for a soft MEX material, thus, PA 12/TPU was studied in the end to check the applicability of this combination for the SLB test. Based on the correlation for the component bending stiffness, which is the product of the moment of inertia and the elastic modulus, the variation of the geometry-based moment of inertia was chosen. Nonetheless, the adaptation of the elastic modulus is possible, but by changing the printing parameters more variables can be affected, making it harder to keep a comparable processing condition.

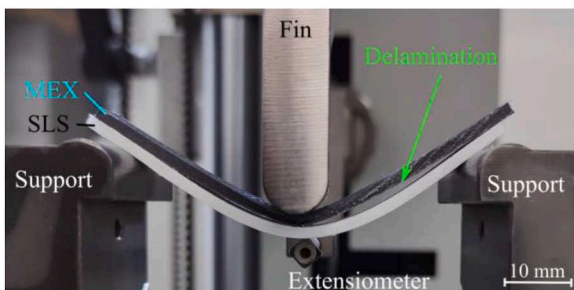


Fig. 3. Completely delaminated MEX layer from SLS layer during flexural test of a PA 12/PACF specimen.

To obtain a qualitative ranking of the processing parameters, the first material combination PA 12/PAGF was produced with different nozzle temperatures, sample thickness, and orientations of the bonding layer. In Fig. 4 the  $G$  for both approaches ( $G_{UC}$  with Eq. (1) and  $G_{SLB}$  with Eq. (2)) are shown for the first material combination. The first obvious trend is the tendency of increased values for higher nozzle temperatures because the MEX (PAGF) strands bond better to the SLS PA 12 (230 °C vs. 250 °C). Another dominant trend is the influence of the thicknesses between SLS and MEX, a thicker PAGF-MEX layer increases the bending stiffness of the whole composite (4.2 vs. 3.3). Depending on which factors were considered in the equation, the effect of the parameters is more ( $G_{UC}$  with Eq. (1)) or less ( $G_{SLB}$  with Eq. (2)) pronounced in the results. Taking the load-displacement curves from Fig. 4b) into account, the impact becomes more visible.  $G_{UC}$  calculated by Eq. (1) only considers the area below the curve divided by the uncracked geometry, thus, leading to higher values. By calculating  $G_{SLB}$  with Eq. (2), the influence of the bending stiffness  $R$  (dependent on the thickness of the composite of each material (Equation 3)) is considered and reduces the bias in the results. In general,  $G_{UC}$  and  $G_{SLB}$  differ significantly in the magnitudes, which can be traced back to purely energy-based calculation of  $G_{UC}$  without any correction factor resulting in an overestimation of the energy release rate. The effect of the bending stiffness is visible in Fig. 5, in which single frames from two representative tests are shown. Samples with 4 mm SLS (4\_2) bend more before the crack starts to grow than the stiffer 3\_3 samples because PAGF is stiffer than PA 12 (compare Table 3). Therefore, if the bending stiffness is not considered during the calculation its effect will be as pronounced as in the  $G_{UC}$  results. Lastly, the impact of the orientation of the first bonding layer, which is either horizontal (h) or vertical (v) and shown in Fig. 1c) and Fig. 5 (interfaces). It is visible that between the deposited strands no particles stick to the MEX surface, because of the oval shape during the deposition. Therefore, the bonding area is not 100% of the overprinted area. Another factor could be the crack's "sharpness" depending on the orientation: the crack is sharper for vertical samples, due to the clear separation with the foil. Horizontal layers have the potential to form dull cracks, depending on the relative alignment of foil and the deposition position of the material. In Fig. 5 (Interfaces) this arrangement-dependent factor is visible: horizontally printed layers can, due to the oval shape of a deposited strand, create an area without contact requiring a new initiation of the crack. This was observed for the crack propagation, which is not considered for this study since it only focussed on the crack initiation.

In general, the scattering of the results was high due to geometrical changes for the SLS parts and the MEX layers, resulting in different bonding qualities for the same parameter setting, and the production by AM. Even though care was taken to only print on similar plate thickness (deviations of max. 0.03 mm), it still had an impact.

With the results from the PA 12/PAGF, the high impact of the samples bending stiffness became clear. Therefore, to focus more on the stiffness effect, the nozzle temperature was not varied for the next material combination, namely PA 12/PACF. Instead, a greater number of different sample thicknesses were produced.

The results for PA 12/PACF are summarised in Fig. 6a) and b) where a rising trend from 2\_1 up to 4\_1 is visible. It resulted from the relatively thin MEX layer (1 mm), which with this thickness was too flexible and allowed high deformations. As stated in Table 1 all MEX structures were printed with 80% infill, resulting in gaps between deposited paths allowing a certain flexibility. Based on the evaluations, with high deformations, the values for  $G$  became higher. With increasing MEX-layer thickness (4\_2, 3\_3, and 2\_4) the calculated energy release rates show a declining effect. This is also visible from the frames in Fig. 6b) of representative samples taken right before the crack started (or at the same moment as for 2\_1) to grow. Thinner bottom layers allow a larger deformation before the crack propagates, at the same time, a thicker upper layer requires more force to create the required deformation for said crack propagation. Therefore, more energy needs to be applied to

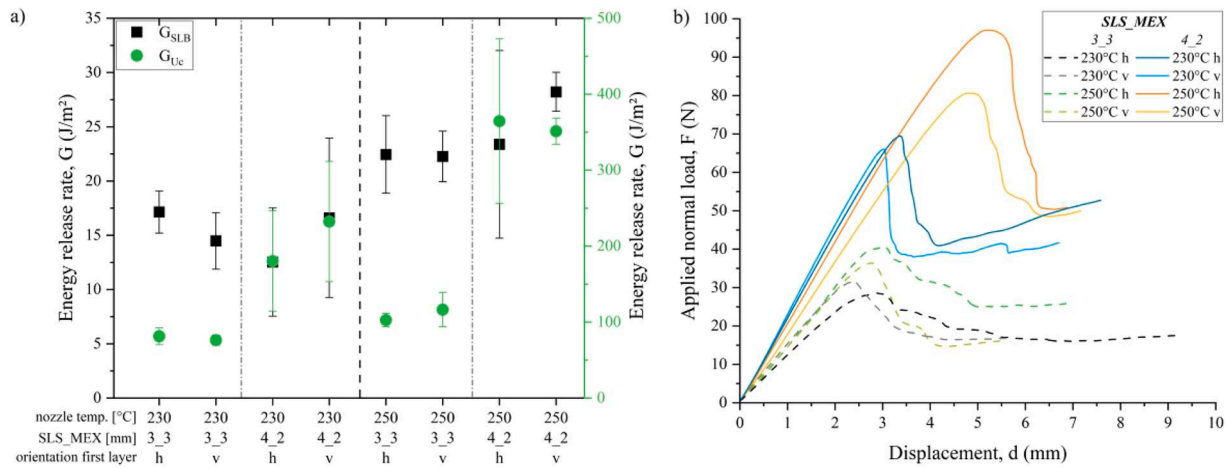


Fig. 4. (a) Energy release rates of PA 12/PAGF with different nozzle temperatures, the thickness of SLS\_MEX (SLS = top layer, MEX = bottom layer), and first layer orientations, (note the different scales for  $G_{UC}$  and  $G_{SLB}$ ) and (b) representative force-displacement curves for all PA 12/PAGF.

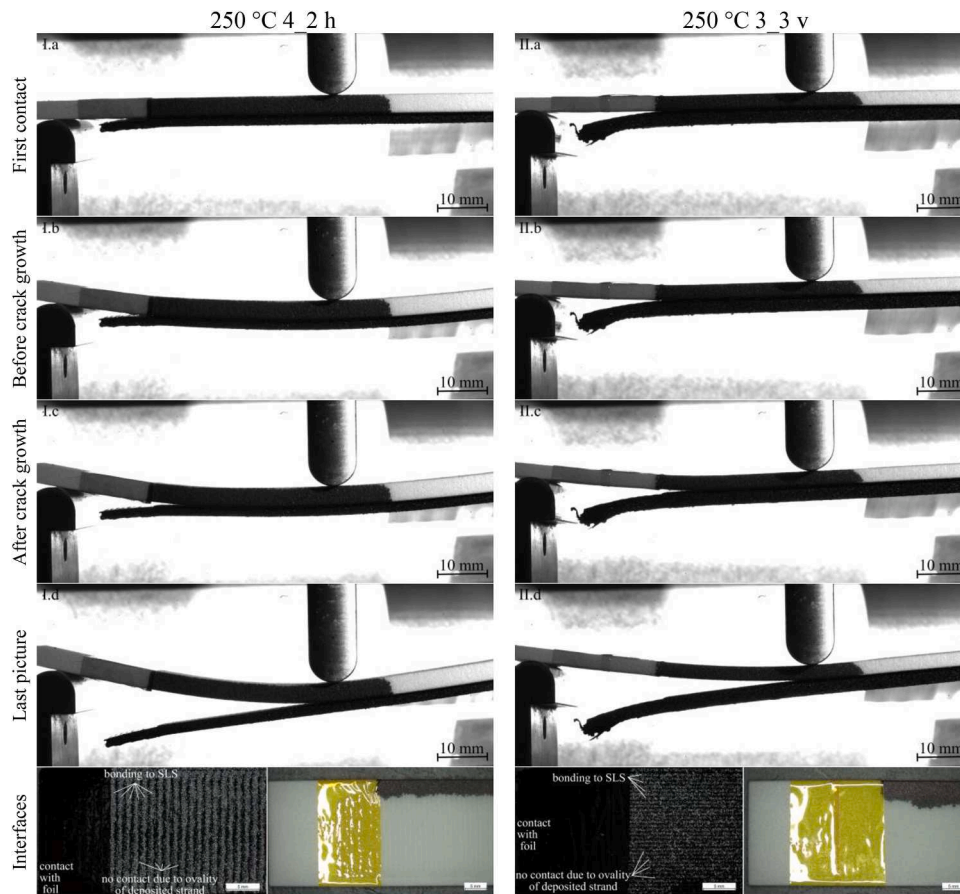


Fig. 5. Selected single frames of PA 12/PAGF and the corresponding interfaces (black = MEX, white = SLS with foil) after testing (black edge comes from marker to have higher contrast to record crack propagation).

detach the more flexible layers. As already mentioned before, the high scattering for the single points of  $G_{SLB}$  limits the significance of the visible trends. Thicker MEX layers in combination with thin SLS layers increase the tendency of warpage and, thus, the internal stresses in the bonding layer. The latter can decrease the bonding strength and explain the low strength for 2\_4 samples [38].

Furthermore, mono-material samples with PACF were produced and the results are presented in Fig. 7a). As for the mixed PACF samples, the same issue occurred if the bottom layer, which is supposed to

delaminate, was “too thin”. With this flexibility, a higher load and/or displacement are required to provoke a crack propagation for detachment. In combination with a stiffer top layer, this led to a higher force to initiate the crack and, therefore, the 4\_1 showed the highest values. In Fig. 7b) a representative sample is shown with some kind of “filament-bridging”. Due to this, the crack did not grow in the desired layer anymore and falsified the result. In addition, the crack propagation was audible but not yet visible, which leads to the conclusion that the crack grew faster in the middle part of the sample than on the outside

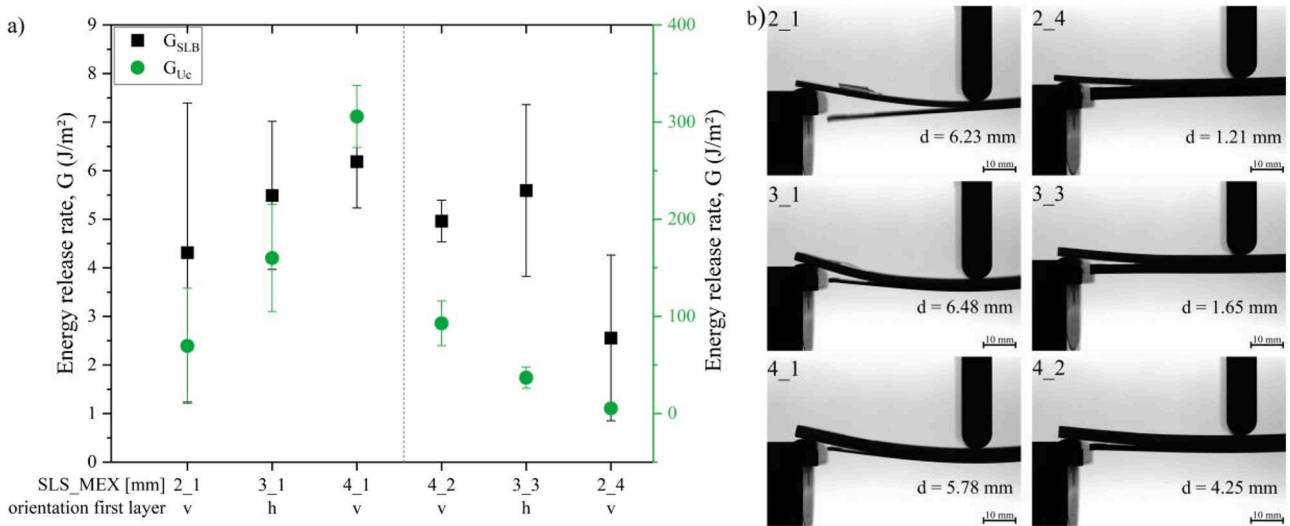


Fig. 6. (a) Energy release rates for PA 12/PACF samples with different thicknesses of SLS\_MEX (SLS = top layer, MEX = bottom layer) and its first layer orientations (note the different scales for  $G_{Uc}$  and  $G_{SLB}$ ) as well as (b) deformation right before crack propagation.

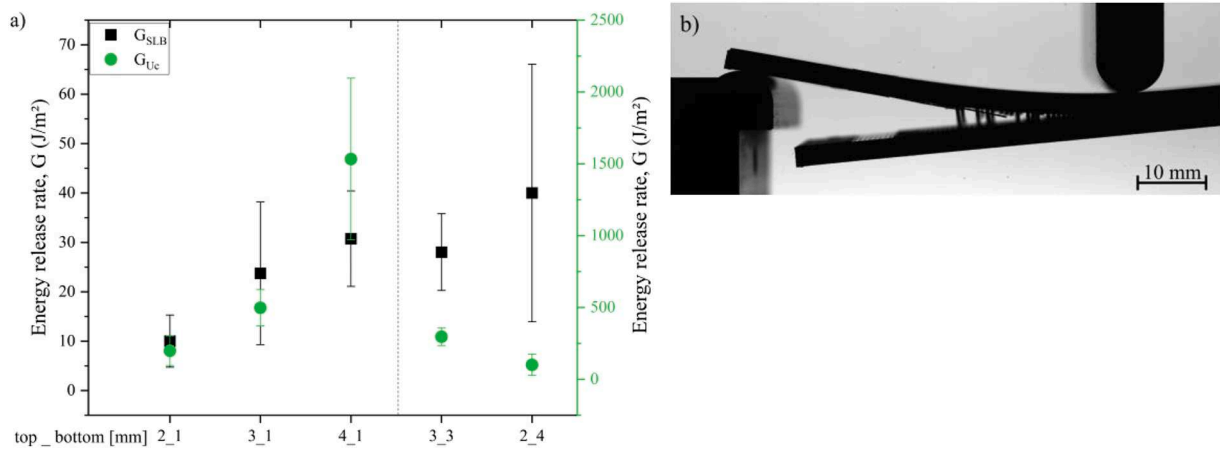


Fig. 7. (a) Evaluation for PACF mono samples with different thicknesses (both MEX) (note the different scales for  $G_{Uc}$  and  $G_{SLB}$ ) and challenges with (b) filament bridging during crack propagation.

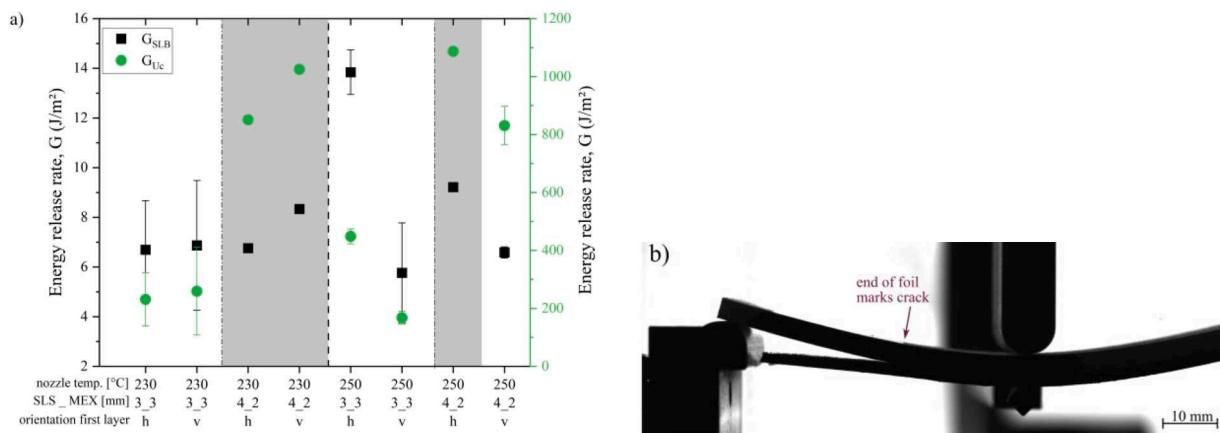


Fig. 8. (a) Energy release rates for PA 12/TPU samples with different nozzle temperatures, thicknesses for SLS\_MEX (SLS = top layer, MEX = bottom layer), and first layer orientations, (note the different scales for  $G_{Uc}$  and  $G_{SLB}$ ) grey marked (b) samples did not create crack propagation.

(perimeter), which was recorded by the camera.

PAGF and PACF (mono and mixed) fulfil the requirement of being stiff enough to initiate a crack between the materials, but this raises the question of whether the SLB approach is still applicable and valid for materials on the other side of the mechanical property spectrum – like a soft TPU – or not. As shown in Table 3, the stiffness of TPU is <10% of the fibre-reinforced PA.

First of all, for TPU not all variations were successfully delaminated due to its flexibility. Parameter settings, which lead to no crack propagation and, therefore, no delamination, are grey-boxed in Fig. 8. Even though no crack initiation took place, the force and displacement at the end of the test – before reaching the ultimate set machine limit – were considered to evaluate the  $G$ -values to gain information about the introduced energy. It can be interpreted as a lower limit, without information about the additional required energy to initiate the crack growth. Mostly 4.2 samples did not delaminate, which had a thinner MEX layer. With this thinner MEX layer, the flexibility of the MEX layer is higher and deforms up to higher deformation without losing the bonding to the SLS plate. An increased number of samples produced with the same processing parameters would lead to similar results. Based on this, the first crucial limitation was found for the SLB test: a certain stiffness is required for the crack initiation. Even a longer initial crack length (from around 20 – 25 mm to over 30 mm) did not solve this challenge, as shown in Fig. 8b). Generally, the machine limit was set to 10 mm deformation – far outside the linear-elastic area of these samples – to avoid slipping of the sample between the supports. In contrast to the stiffer PA 12/PAGF or PA 12/PACF samples, delaminating PA 12/TPU samples showed no clear trend for the nozzle temperature, but the thicknesses for  $G_{Uc}$ . The latter can be explained as before: the utilized calculation did not consider the bending stiffness and, thus, has higher  $G$ -values with this evaluation. Lastly, the orientations of the bonding layers seem to have no clear trend; for specimens printed at 230 °C, the  $G$ -values are almost equal, while for specimens printed at 250 °C a horizontal orientation leads to higher  $G$ -values than vertically printed ones. This does not include the invalid grey-marked tests. Thicker TPU layers, which added up to 6 mm with the PA 12 SLS plate (2 mm SLS plate and 4 mm TPU layer), could also not be delaminated for any printing temperature or orientation.

#### 4. Conclusions

Within this study, methodological knowledge of the literature already published single leg bending (SLB) tests was applied and compared to different material combinations, which was not yet done in the literature. A selectively sintered polyamide 12 was successfully imprinted by MEX with reinforced PA 12 (with glass fibres and carbon fibres) and with a thermoplastic polyurethane (TPU). By using different materials (fibre-reinforced vs. TPU) the impact of diverging mechanical properties on the test method was investigated. The chosen combinations bonded sufficiently to each other to be tested. The results within one composite were ranked regarding parameters such as the influence of nozzle temperatures, sample thickness (which defines the bending stiffness), and partially the orientation of the bonding layer. Nevertheless, we faced certain limitations such as the required stiffness to initiate a crack. This issue occurs when the material is either too flexible or too thin, resulting in insufficient bending stiffness to initiate crack growth. Certain trends, such as the impact of the nozzle temperature can be ranked, but no absolute numerical comparison can be drawn. In the case of a stronger interface bonding than the inter- and intralayer bonding strength, the crack grows out-of-plane and is invalid for evaluation.

Furthermore, it has to be considered that the quality of additively manufactured samples varies depending on the repeatability of the production, filament quality, printer, operator and many more. One advantage is the easier production of the samples which does not require any glueing, as for Double Cantilever Beam, and for a first ranking of bonding strength with an initial crack even without a camera system.

However, the SLB test setup leads to failure in mixed mode (mode I and mode II) making a direct comparison to other methods complicated. For stiff material combinations, the approach is suitable, while for the combination of relative soft-hard, it is questionable if the calculations are still applicable. Based on the results other factors or test geometries should be considered. Nonetheless, for stiff AM components/combinations a relative ranking of printing parameters is possible.

For further investigation, more processing and testing parameters will be considered to determine their impact on the mechanical properties and subsequently on the bonding strength. Furthermore, a focus will be on the critical bending stiffness ( $R$ ) of the sample for the SLB test geometry to gain more knowledge about the limiting factors of this test method. For flexible material combinations such as TPU, a change of geometry, such as a longer and thinner specimen, could enable a larger deformation, leading to higher stresses in the bonding layer and ideally to delamination. Another possible optimisation is a pre-crack placed closer to the fin to introduce higher stresses.

#### CRediT authorship contribution statement

**T. Stiller:** Writing – review & editing, Writing – original draft, Visualization, Validation, Methodology, Investigation, Formal analysis, Data curation, Conceptualization. **R.C. Kerschbaumer:** Writing – review & editing, Project administration, Methodology, Funding acquisition. **C. Waly:** Writing – review & editing, Validation, Methodology, Conceptualization. **B. Zink:** Writing – review & editing, Validation, Methodology. **J. Slapnik:** Writing – review & editing, Validation, Methodology. **G. Pinter:** Writing – review & editing, Validation, Supervision, Resources, Methodology, Conceptualization.

#### Declaration of competing interest

The authors declare that they have no known competing financial interests or personal relationships that could have appeared to influence the work reported in this paper.

#### Acknowledgements

The research work of this paper was performed at the Polymer Competence Center Leoben GmbH (PCCL, Austria) within the framework of the funding program “Production of the Future” of the Federal Ministry for Climate Action, Environment, Energy, Mobility, Innovation and Technology and the Federal Ministry for Digital and Economic Affairs in the project “RFIDinSLS” with contributions by Joanneum Research Forschungsgesellschaft mbH, Kronowetter GmbH, and RPD Rapid Product Development GmbH. The PCCL is funded by the Austrian Government and the State Governments of Styria, Lower Austria and Upper Austria. Furthermore, this research was funded by the Horizon Europe Framework Programme and the call HORIZON-WIDERA-2021-ACCESS03, under the grant agreement for project 101079051 – IPPT\_TWINN.

#### Data availability

Data will be made available on request.

#### References

- [1] S. Scott Crump US5121329A.
- [2] ISO/ASTM52900:2021, ISO/ASTM 52900:2021 - Additive manufacturing - General principles - Fundamentals and vocabulary.
- [3] T. Barši Palmič, J. Slavič, M. Boltežar, Process Parameters for FFF 3D-Printed Conductors for Applications in Sensors, Sensors (Basel) (2020) 20, <https://doi.org/10.3390/s20164542>.
- [4] Y. Ibrahim, A. Elkholy, J.S. Schofield, G.W. Melenka, R. Kempers, Effective thermal conductivity of 3D-printed continuous fiber polymer composites, Adv. Manuf. 6 (2020) 17–28, <https://doi.org/10.1080/20550340.2019.1710023>.

- [5] A. Yadav, P. Rohru, A. Babbar, R. Kumar, N. Ranjan, J.S. Chohan, R. Kumar, M. Gupta, Fused filament fabrication: a state-of-the-art review of the technology, materials, properties and defects, *Int. J. Interact. Des. Manuf.* 17 (2023) 2867–2889, <https://doi.org/10.1007/s12008-022-01026-5>.
- [6] L.J. Tan, W. Zhu, K. Zhou, Recent Progress on Polymer Materials for Additive Manufacturing, *Adv. Funct. Materials* 30 (2020) 2003062, <https://doi.org/10.1002/adfm.202003062>.
- [7] A. Pilipović, T. Brajlili, I. Drstvenšek, Influence of Processing Parameters on Tensile Properties of SLS Polymer Product, *Polymers (Basel)* 10 (2018), <https://doi.org/10.3390/polym10111208>.
- [8] M. Harris, J. Potgieter, R. Archer, K.M. Arif, Effect of Material and Process Specific Factors on the Strength of Printed Parts in Fused Filament Fabrication: a Review of Recent Developments, *Materials (Basel)* 12 (2019), <https://doi.org/10.3390/ma12101664>.
- [9] A. Lepoivre, N. Boyard, A. Levy, V. Sobotka, Heat Transfer and Adhesion Study for the FFF Additive Manufacturing Process, *Procedia Manufacturing* 47 (2020) 948–955, <https://doi.org/10.1016/j.promfg.2020.04.291>.
- [10] F. Bähr, E. Westkämper, Correlations between Influencing Parameters and Quality Properties of Components Produced by Fused Deposition Modeling, *Procedia CIRP* 72 (2018) 1214–1219, <https://doi.org/10.1016/j.procir.2018.03.048>.
- [11] U. Gulzar, C. Glynn, C. O'Dwyer, Additive manufacturing for energy storage: methods, designs and material selection for customizable 3D printed batteries and supercapacitors, *Curr. Opin. Electrochem.* 20 (2020) 46–53, <https://doi.org/10.1016/j.coelec.2020.02.009>.
- [12] Y. Pang, Y. Cao, Y. Chu, M. Liu, K. Snyder, D. MacKenzie, C. Cao, Additive Manufacturing of Batteries, *Adv. Funct. Materials* 30 (2020) 1906244, <https://doi.org/10.1002/adfm.201906244>.
- [13] M. Fleisch, A. Thalhamer, G. Meier, P.A.F. Huber, P.F. Fuchs, G. Pinter, S. Schlögl, M. Berer, Chiral-based mechanical metamaterial with tunable normal-strain shear coupling effect, *Eng. Struct.* 284 (2023) 115952, <https://doi.org/10.1016/j.engstruct.2023.115952>.
- [14] E. Truszkiewicz, A. Thalhamer, M. Rossegger, M. Vetter, G. Meier, E. Rossegger, P. Fuchs, S. Schlögl, M. Berer, Mechanical behavior of 3D -printed polymeric metamaterials for lightweight applications, *J. Appl. Polymer Sci.* 139 (2022) 51618, <https://doi.org/10.1002/app.51618>.
- [15] I. Raguz, M. Berer, M. Fleisch, C. Holzer, J. Brancart, B. Vanderborcht, S. Schlögl, Soft dielectric actuator produced by multi-material fused filament fabrication 3D printing, *Polymers Adv. Tech.* 34 (2023) 1967–1978, <https://doi.org/10.1002/pat.6024>.
- [16] T.C. Dzogbewu, N. Amoah, S. Afrifa Jnr, S.K. Fianko, D.J. de Beer, Multi-material additive manufacturing of electronics components: a bibliometric analysis, *Results Eng.* 19 (2023) 101318, <https://doi.org/10.1016/j.rineng.2023.101318>.
- [17] J. Persad, S. Rocke, Multi-material 3D printed electronic assemblies: a review, *Results Eng.* 16 (2022) 100730, <https://doi.org/10.1016/j.rineng.2022.100730>.
- [18] T. Stiller, M. Berer, A.K. Katta, B. Haar, E. Truszkiewicz, W. Kraschitzer, H. Stepanovsky, G. Pinter, J.M. Lackner, Powder ageing of Polyamide 6 in laser sintering and its effects on powder and component characteristics, *Addit. Manuf.* 58 (2022) 102987, <https://doi.org/10.1016/j.addma.2022.102987>.
- [19] P.C. Gomes, O.G. Piñeiro, A.C. Alves, O.S. Carneiro, On the Reuse of SLS Polyamide 12 Powder, *Materials (Basel)* 15 (2022), <https://doi.org/10.3390/ma15165486>.
- [20] A. Gazzerò, W. Polini, L. Sorrentino, G. Giuliano, Aging of PA12 Powder in Powder Bed Fusion, *Appl. Sci.* 13 (2023) 5599, <https://doi.org/10.3390/app13095599>.
- [21] O.A. Alo, I.O. Otunniyi, D. Mauchline, Effects of reuse on morphology, size and shape distributions of PA 12 powder in selective laser sintering and quality of printed parts, *J. Polym. Res.* 30 (2023), <https://doi.org/10.1007/s10965-022-03423-6>.
- [22] D. Fico, D. Rizzo, R. Casciaro, C. Esposito Corcione, A Review of Polymer-Based Materials for Fused Filament Fabrication (FFF): focus on Sustainability and Recycled Materials, *Polymers (Basel)* 14 (2022), <https://doi.org/10.3390/polym14030465>.
- [23] C. Kalinke, R.D. Crapnell, P.R. de Oliveira, B.C. Janegitz, J.A. Bonacin, C.E. Banks, How to Improve Sustainability in Fused Filament Fabrication (3D Printing) Research? Global Challenges (2024) 2300408 <https://doi.org/10.1002/gch2.202300408>.
- [24] K. Mikula, D. Skrzypczak, G. Izydorczyk, J. Warchol, K. Moustakas, K. Chojnacka, A. Witek-Krowiak, 3D printing filament as a second life of waste plastics-a review, *Environ. Sci. Pollut. Res. Int.* 28 (2021) 12321–12333, <https://doi.org/10.1007/s11356-020-10657-8>.
- [25] X. Gao, S. Qi, X. Kuang, Y. Su, J. Li, D. Wang, Fused filament fabrication of polymer materials: a review of interlayer bond, *Addit. Manuf.* 37 (2021) 101658, <https://doi.org/10.1016/j.addma.2020.101658>.
- [26] C. Waly, S. Petersmann, F. Arbeiter, Crack penetration versus deflection in extrusion-based additive manufacturing – Impact of nozzle temperature and morphology, *Theor. Appl. Fract. Mech.* 127 (2023) 104032, <https://doi.org/10.1016/j.tafmec.2023.104032>.
- [27] C. Waly, S. Petersmann, F. Arbeiter, Multimaterial Extrusion-Based Additive Manufacturing of Compliant Crack Arresters: influence of Interlayer Length, Thickness, and Applied Strain Rate, *Adv. Eng. Mater.* 25 (2023) 2101703, <https://doi.org/10.1002/adem.202101703>.
- [28] N. Maqsood, M. Rimašauskas, Delamination observation occurred during the flexural bending in additively manufactured PLA-short carbon fiber filament reinforced with continuous carbon fiber composite, *Res. Eng.* 11 (2021) 100246, <https://doi.org/10.1016/j.rineng.2021.100246>.
- [29] C.S. Davis, K.E. Hillgartner, S.H. Han, J.E. Seppala, Mechanical strength of welding zones produced by material extrusion additive manufacturing, *Addit. Manuf.* 16 (2017) 162–166, <https://doi.org/10.1016/j.addma.2017.06.006>.
- [30] J. Fonseca, L.A. Ferreira, M. de Moura, M. Machado, J.L. Alves, Study of the interlaminar fracture under mode I loading on FFF printed parts, *Compos. Struct.* 214 (2019) 316–324, <https://doi.org/10.1016/j.compstruct.2019.02.005>.
- [31] M. Spoerk, F. Arbeiter, H. Cajner, J. Sapkota, C. Holzer, Parametric optimization of intra- and inter-layer strengths in parts produced by extrusion-based additive manufacturing of poly(lactic acid), *J. Appl. Polymer Sci.* 134 (2017) 45401, <https://doi.org/10.1002/app.45401>.
- [32] D. Young, N. Wetmore, M. Czabaj, Interlayer fracture toughness of additively manufactured unreinforced and carbon-fiber-reinforced acrylonitrile butadiene styrene, *Addit. Manuf.* 22 (2018) 883–890, <https://doi.org/10.1016/j.addma.2018.02.010>.
- [33] M.Qamar Tanveer, G. Mishra, S. Mishra, R. Sharma, Effect of infill pattern and infill density on mechanical behaviour of FDM 3D printed Parts- a current review, *Mater. Today* 62 (2022) 100–108, <https://doi.org/10.1016/j.matpr.2022.02.310>.
- [34] A. Forés-Garriga, M.A. Pérez, G. Gómez-Gras, G. Reyes-Pozo, Role of infill parameters on the mechanical performance and weight reduction of PEI Ultem processed by FFF, *Mater. Des.* 193 (2020) 108810, <https://doi.org/10.1016/j.matdes.2020.108810>.
- [35] A. García-Collado, J.M. Blanco, M.K. Gupta, R. Dorado-Vicente, Advances in polymers based Multi-Material Additive-Manufacturing Techniques: state-of-art review on properties and applications, *Addit. Manuf.* 50 (2022) 102577, <https://doi.org/10.1016/j.addma.2021.102577>.
- [36] U. Shaikat, E. Rossegger, S. Schlögl, A Review of Multi-Material 3D Printing of Functional Materials via Vat Photopolymerization, *Polymers (Basel)* 14 (2022), <https://doi.org/10.3390/polym14122449>.
- [37] M. Fleisch, A. Thalhamer, G. Meier, P.F. Fuchs, G. Pinter, S. Schlögl, M. Berer, Asymmetric chiral and antichiral mechanical metamaterials with tunable Poisson's ratio, *APL Mater.* 10 (2022) 061105, <https://doi.org/10.1063/5.0091756>.
- [38] J. Slapnik, R. Lorber, I. Pulko, M. Huskić, K.P. Crešnar, Overprinting of TPU onto PA6 Substrates: the Influences of the Interfacial Area, Surface Roughness and Processing Parameters on the Adhesion between Components, *Polymers (Basel)* 16 (2024), <https://doi.org/10.3390/polym16050650>.
- [39] M.F. Rabbi, V. Chalivendra, Interfacial fracture characterization of multi-material additively manufactured polymer composites, *Composites Part C* 5 (2021) 100145, <https://doi.org/10.1016/j.jcocom.2021.100145>.
- [40] T.S. Lumpe, J. Mueller, K. Shea, Tensile properties of multi-material interfaces in 3D printed parts, *Mater. Des.* 162 (2019) 1–9, <https://doi.org/10.1016/j.matdes.2018.11.024>.
- [41] A. Ghimire, P.-Y. Chen, Mechanical properties of additively manufactured multi-material stiff-soft interfaces: guidelines to manufacture complex interface composites with tunable properties, *Mater. Des.* 238 (2024) 112677, <https://doi.org/10.1016/j.matdes.2024.112677>.
- [42] A. Khudiakova, F. Arbeiter, M. Spoerk, M. Wolfahrt, D. Godec, G. Pinter, Inter-layer bonding characterisation between materials with different degrees of stiffness processed by fused filament fabrication, *Addit. Manuf.* 28 (2019) 184–193, <https://doi.org/10.1016/j.addma.2019.05.006>.
- [43] T. Stiller, A. Hausberger, M. Berer, A.M. Schwan, A. Hinterer, S. Spalt, G. Pinter, J. M. Lackner, Determination of Cyclic Load Limits for Plasma-Sprayed Copper Tracks on Material Extrusion-Based Printed Surfaces, *Adv. Eng. Mater.* 25 (2023) 2200567, <https://doi.org/10.1002/adem.202200567>.
- [44] J. Wiener, Biomimetic concepts for the optimization of mechanical properties in layered polymeric materials, 2023.
- [45] B.D. Davidson, V. Sundararaman, A single leg bending test for interfacial fracture toughness determination, *Int. J. Fracture* 78 (1996) 193–210.
- [46] L.Da Silva, V. Esteves, F. Chaves, Fracture toughness of a structural adhesive under mixed mode loadings, *Materialwissenschaft Werkst* 42 (2011) 460–470, <https://doi.org/10.1002/mawe.201100808>.
- [47] B.D. Davidson, A. Bansal, Q. Bing, X. Sun, Geometrically Nonlinear Determination of Energy Release Rate and Mode Ratio in Single Leg Bending Tests, *J. Reinforced Plast. Compos.* 28 (2009) 1881–1901, <https://doi.org/10.1177/0731684408089235>.
- [48] B.D. Davidson, R. Krüger, M. König, Three-dimensional analysis of center delaminated unidirectional and multidirectional single-leg bending specimens, *Compos. Sci. Technol.* 54 (1995) 385–394.
- [49] S. Hashemi, A.J. Kinloch, J.G. Williams, The analysis of interlaminar fracture in uniaxial fibre-polymer composites, *Proc. R. Soc. Lond. A* 427 (1990) 173–199, <https://doi.org/10.1098/rspa.1990.0007>.
- [50] F.M. Ramirez, M.F. de Moura, R.D. Moreira, F.G. Silva, Experimental and numerical mixed-mode I + II fracture characterization of carbon fibre reinforced polymer laminates using a novel strategy, *Compos. Struct.* 263 (2021) 113683, <https://doi.org/10.1016/j.compstruct.2021.113683>.
- [51] D.-K. Shin, J.-J. Lee, J.-S. Hawong (Eds.), Measurement of thin film adhesion by single cantilever beam method equipped with adjustable jig, 2014.
- [52] A. Szekrényes, J-integral for delaminated beam and plate models, *Mech. Eng.* 56 (2012) 63–71.
- [53] DIN EN ISO 11357:2009 - Kunststoffe – Dynamische Differenz-Thermoanalyse (DSC).
- [54] ISO178:2010, DIN EN ISO 178:2010 Kunststoffe- Bestimmung der Biegeeigenschaften.
- [55] ISO 13586:2018 - Plastics - Determination of fracture toughness (Gic and Kic) - Linear elastic fracture mechanics (LEFM) approach.
- [56] ASTM D5045-14(2022) - Standard test methods for plane-strain fracture toughness and strain energy release rate of plastic materials.

- [57] A. Saiani, W.A. Daunch, H. Verbeke, J.-W. Leenslag, J.S. Higgins, Origin of Multiple Melting Endotherms in a High Hard Block Content Polyurethane. 1. Thermodynamic Investigation, *Macromolecules* 34 (2001) 9059–9068, <https://doi.org/10.1021/ma0105993>.
- [58] A. Frick, A. Rochman, Characterization of TPU-elastomers by thermal analysis (DSC), *Polym. Test* 23 (2004) 413–417, <https://doi.org/10.1016/j.polymertesting.2003.09.013>.
- [59] S.F. Costa, F.M. Duarte, J.A. Covas, Estimation of filament temperature and adhesion development in fused deposition techniques, *J. Mater. Process. Technol.* 245 (2017) 167–179, <https://doi.org/10.1016/j.jmatprotec.2017.02.026>.
- [60] C. Luo, Modeling the temperature profile of an extrudate in material extrusion additive manufacturing, *Mater. Lett.* 270 (2020) 127742, <https://doi.org/10.1016/j.matlet.2020.127742>.
- [61] J.E. Mark, *Physical Properties of Polymers Handbook*, 2nd. ed, Springer Science+Business Media LLC, New York, NY, 2007.
- [62] D. Ravoori, C. Lowery, H. Prajapati, A. Jain, Experimental and theoretical investigation of heat transfer in platform bed during polymer extrusion based additive manufacturing, *Polym. Test* 73 (2019) 439–446, <https://doi.org/10.1016/j.polymertesting.2018.11.025>.
- [63] L.R. Lopes, A.F. Silva, O.S. Carneiro, Multi-material 3D printing: the relevance of materials affinity on the boundary interface performance, *Addit. Manufact.* 23 (2018) 45–52, <https://doi.org/10.1016/j.addma.2018.06.027>.
- [64] G.D. Goh, Y.L. Yap, S. Agarwala, W.Y. Yeong, Recent Progress in Additive Manufacturing of Fiber Reinforced Polymer Composite, *Adv. Mater. Technol.* 4 (2019) 1800271, <https://doi.org/10.1002/admt.201800271>.
- [65] G. Liao, Z. Li, Y. Cheng, D. Xu, D. Zhu, S. Jiang, J. Guo, X. Chen, G. Xu, Y. Zhu, Properties of oriented carbon fiber/polyamide 12 composite parts fabricated by fused deposition modeling, *Mater. Des.* 139 (2018) 283–292, <https://doi.org/10.1016/j.matdes.2017.11.027>.
- [66] G.D. Goh, Y.L. Yap, H.K.J. Tan, S.L. Sing, G.L. Goh, W.Y. Yeong, Process–Structure–Properties in Polymer Additive Manufacturing via Material Extrusion: a Review, *Crit. Rev. Solid State Mater. Sci.* 45 (2020) 113–133, <https://doi.org/10.1080/10408436.2018.1549977>.
- [67] G. Gómez-Gras, M.D. Abad, M.A. Pérez, Mechanical Performance of 3D-Printed Biocompatible Polycarbonate for Biomechanical Applications, *Polymers (Basel)* 13 (2021), <https://doi.org/10.3390/polym13213669>.
- [68] K.M. Rahman, T. Letcher, R. Reese (Eds.), *Mechanical Properties of Additively Manufactured PEEK Components Using Fused Filament Fabrication*, 2015.
- [69] C. Benwood, A. Anstey, J. Andrzejewski, M. Misra, A.K. Mohanty, Improving the Impact Strength and Heat Resistance of 3D Printed Models: structure, Property, and Processing Correlations during Fused Deposition Modeling (FDM) of Poly (Lactic Acid), *ACS Omega* 3 (2018) 4400–4411, <https://doi.org/10.1021/acsomega.8b00129>.
- [70] S. Petersmann, P. Spoerk-Erdely, M. Feuchter, T. Wieme, F. Arbeiter, M. Spoerk, Process-induced morphological features in material extrusion-based additive manufacturing of polypropylene, *Addit. Manufact.* 35 (2020) 101384, <https://doi.org/10.1016/j.addma.2020.101384>.
- [71] H. Dominghaus, P. Elsner, P. Eyerer, T. Hirth, *Kunststoffe*, Springer Berlin Heidelberg, Berlin, Heidelberg, 2012.
- [72] W. Grellmann, *Kunststoffprüfung*, 2nd ed, Hanser, München, 2011.
- [73] G. Ehrenstein, *Polymer-Werkstoffe: struktur; Eigenschaften; Anwendung*, third. Aufl, Carl Hanser Fachbuchverlag (s.l) (2011).
- [74] J. Chen, S.J. Bull, Approaches to investigate delamination and interfacial toughness in coated systems: an overview, *J. Phys. D* 44 (2011) 34001, <https://doi.org/10.1088/0022-3727/44/3/034001>.